

## Reducing flicker noise in chemical vapor deposition graphene field-effect transistors

Heather N. Arnold,<sup>1,a)</sup> Vinod K. Sangwan,<sup>1,a)</sup> Scott W. Schmucker,<sup>2</sup> Cory D. Cress,<sup>3</sup> Kyle A. Luck,<sup>1</sup> Adam L. Friedman,<sup>4</sup> Jeremy T. Robinson,<sup>3</sup> Tobin J. Marks,<sup>1,5</sup> and Mark C. Hersam<sup>1,5,6,b)</sup>

<sup>1</sup>Department of Materials Science and Engineering, Northwestern University, Evanston, Illinois 60208, USA

<sup>2</sup>National Research Council Post Doctoral Fellow, Residing at the U. S. Naval Research Laboratory, Washington, D.C. 20375, USA

<sup>3</sup>Electronics Science and Technology Division, U. S. Naval Research Laboratory, Washington, D.C. 20375, USA

<sup>4</sup>Materials Science Division, U. S. Naval Research Laboratory, Washington, D.C. 20375, USA

<sup>5</sup>Department of Chemistry, Northwestern University, Evanston, Illinois 60208, USA

<sup>6</sup>Department of Medicine, Northwestern University, Evanston, Illinois 60208, USA

(Received 15 November 2015; accepted 9 February 2016; published online 18 February 2016)

Single-layer graphene derived from chemical vapor deposition (CVD) holds promise for scalable radio frequency (RF) electronic applications. However, prevalent low-frequency flicker noise ( $1/f$  noise) in CVD graphene field-effect transistors is often up-converted to higher frequencies, thus limiting RF device performance. Here, we achieve an order of magnitude reduction in  $1/f$  noise in field-effect transistors based on CVD graphene transferred onto silicon oxide substrates by utilizing a processing protocol that avoids aqueous chemistry after graphene transfer. Correspondingly, the normalized noise spectral density ( $10^{-7}$ – $10^{-8}$   $\mu\text{m}^2 \text{Hz}^{-1}$ ) and noise amplitude ( $4 \times 10^{-8}$ – $10^{-7}$ ) in these devices are comparable to those of exfoliated and suspended graphene. We attribute the reduction in  $1/f$  noise to a decrease in the contribution of fluctuations in the scattering cross-sections of carriers arising from dynamic redistribution of interfacial disorder. © 2016 AIP Publishing LLC.

[<http://dx.doi.org/10.1063/1.4942468>]

Graphene, an atomically thin, two-dimensional honeycomb lattice of  $\text{sp}^2$  carbon atoms, is a promising material for future radio frequency (RF) electronic applications due to its high intrinsic carrier mobility, high cutoff frequency, high saturation velocity, and ideal thickness for ultimate scaling.<sup>1,2</sup> Although micromechanical exfoliation of graphene from graphite has been effective for prototype RF studies,<sup>3</sup> a robust large-area graphene synthesis technique is necessary for practical applications. Towards this end, chemical vapor deposition (CVD) has emerged as a leading pathway to wafer-scale continuous films of single-layer graphene, but devices fabricated from CVD graphene frequently suffer from defects, grain boundaries, wrinkles, and thickness variations. The defects and disorder in CVD graphene compromise intrinsic properties such as carrier mobility and, ultimately, limit the resulting device metrics.<sup>5</sup> Recently, the electronic performance of CVD graphene has improved with incremental advances in growth approaches and through the use of alternative dielectric substrates.<sup>4,5</sup> However, in contrast to the water-free processing of exfoliated graphene devices by e-beam lithography, CVD graphene devices are commonly fabricated using photolithography that includes aqueous processing steps.<sup>6,7</sup> Therefore, it remains unclear whether the limited performance of CVD graphene is attributable to inferior intrinsic material quality or extrinsic impurities introduced during wet transfer and subsequent photolithographic processing.

One device metric that is particularly sensitive to both short-range and long-range disorder is low-frequency flicker noise ( $1/f$  noise). Flicker noise is a limiting factor in CVD graphene applications, because reduced carrier mobility leads to increase in noise amplitude, and the two-dimensional “all-surface” topology is exceptionally sensitive to environmental perturbations.<sup>8,9</sup> Moreover, flicker noise can be up-converted to higher frequencies by the inherent nonlinearities in field-effect transistors (FETs) and circuits, thus limiting the cutoff frequency in RF applications. The behavior of low-frequency noise in exfoliated graphene devices has been extensively studied, and several methods have been developed to reduce noise, such as the fabrication of suspended channels,<sup>10</sup> graded thickness graphene contacts,<sup>11</sup> and screening underlying trap charges *via* few-layer graphene channels.<sup>12</sup> In comparison, relatively few studies have examined  $1/f$  noise in CVD graphene. In these reports, the noise in CVD graphene has been found to be at least one order of magnitude larger than in exfoliated/suspended graphene, presumably due to increased disorder from growth and/or device processing.<sup>13–15</sup>

Here, we conduct a thorough, systematic study of  $1/f$  noise in CVD graphene and report an ultralow noise spectral density (area normalized) of  $10^{-7}$ – $10^{-8}$   $\mu\text{m}^2 \text{Hz}^{-1}$  that is comparable to high-quality exfoliated graphene.<sup>8</sup> The unusual linear energy dispersion in single-layer graphene results in a unique dependence of the  $1/f$  noise characteristics on carrier density. For example, we observe V-shape, M-shape,  $\Lambda$ -shape, or weak/no-shape dependencies of the noise on carrier concentration, which varies with sample quality and processing conditions.<sup>8</sup> Our highest performing CVD graphene devices show an M-shape dependence

<sup>a)</sup>H. N. Arnold and V. K. Sangwan contributed equally to this work.

<sup>b)</sup>Author to whom correspondence should be addressed. Electronic mail: m-hersam@northwestern.edu.

on carrier density that has been previously observed only in high-quality exfoliated graphene,<sup>13,16–19</sup> bilayer graphene,<sup>13</sup> and suspended graphene.<sup>13</sup> This M-shape dependence reveals significant reduction in the dynamic rearrangement of interfacial disorder and is ultimately attributed to the elimination of aqueous processing steps after graphene transfer.

Single-layer graphene was produced by a low-pressure CVD process on enclosed packets of polycrystalline Cu foil.<sup>20</sup> The graphene films were transferred onto 250 nm of thermal SiO<sub>2</sub>/Si substrates *via* wet-chemical processing, which includes a protective layer of poly(methyl methacrylate) (PMMA) and APS 100 copper etchant (Transene Company, Inc.).<sup>21</sup> Prior to etching, PMMA-coated Cu is floated for 3 min in 10% nitric acid to remove graphene from the obverse side of the foil, and the APS etchant is oxygenated to minimize carbonaceous residues after PMMA removal.<sup>21</sup> Following graphene transfer, FETs are fabricated using a procedure tailored to avoid aqueous processing. First, graphene sheets are patterned into 2-probe device geometries using a 495 PMMA A6 resist (MicroChem Inc.) and a contact aligner by deep ultraviolet (DUV) lithography (254 nm). After a reactive ion etch (90 W oxygen plasma), contacts are patterned in a double-layer of 495 PMMA A6 and 950 PMMA A2 resist and developed in 2:1 isopropanol (IPA)/methyl isobutyl ketone (MIBK) solution. Finally, metal evaporation (20 nm Ti/200 nm Au) and non-aqueous lift-off steps are completed. These resist chemistries and processing steps are selected to avoid exposing devices to water subsequent to the initial graphene transfer. Most common photoresists employ water-based developers (often tetramethylammonium hydroxide, KOH, or NaOH in water), leading to contamination of the graphene-SiO<sub>2</sub> interface and occasional delamination of graphene films. In contrast, graphene films in this work were exposed only to MIBK/IPA developers and solvents (acetone and isopropyl alcohol) during and subsequent to removal of the PMMA protective layer. Atomic force microscopy of the resulting graphene FETs (G-FETs) reveals clean graphene surfaces with rms roughness of  $\sim 0.5$  nm (see Figure S1 in the supplementary materials<sup>22</sup>).

All transport and  $1/f$  noise measurements were carried out in vacuum (pressure  $< 10^{-5}$  Torr) using protocols described previously.<sup>23</sup> Transfer characteristics (resistance  $R$  versus gate voltage  $V_g$ ) were acquired (Figure 1(a)) at low drain biases ( $V_d = 0.1$ – $0.3$  V) using highly doped Si as the global back gate. Additionally, the output characteristics (drain current  $I_d$  versus  $V_d$ ) revealed that the devices operate in the linear region for  $|V_d| < 0.8$  V (Figure 1(b)). From these measurements, the charge neutrality point (i.e., Dirac voltage,  $V_{\text{Dirac}}$ ) of the G-FETs was extracted and found to fall in a range between 3 and 25 V (see Figure S2(a) in the supplementary materials<sup>22</sup>). Subsequent field-effect mobility calculations<sup>24</sup> of all 10 devices revealed electron mobility ( $\mu_{\text{FEe}}$ ) in the range of 700–1970 cm<sup>2</sup>/V s (average  $\mu_{\text{FEe}} = 1160$  cm<sup>2</sup>/V s) and hole mobility ( $\mu_{\text{FEh}}$ ) in the range of 1000–3400 cm<sup>2</sup>/V s (average  $\mu_{\text{FEh}} = 2240$  cm<sup>2</sup>/V s), as shown in Figure S2(b) and S2(c), respectively, in the supplementary materials.<sup>22</sup>

Raman spectroscopy was further used to characterize the G-FETs, as shown in Figure 1(c). Measurements were conducted in ambient using a confocal Raman system with 488 nm excitation and a 50 $\times$  objective (NA = 0.65). The

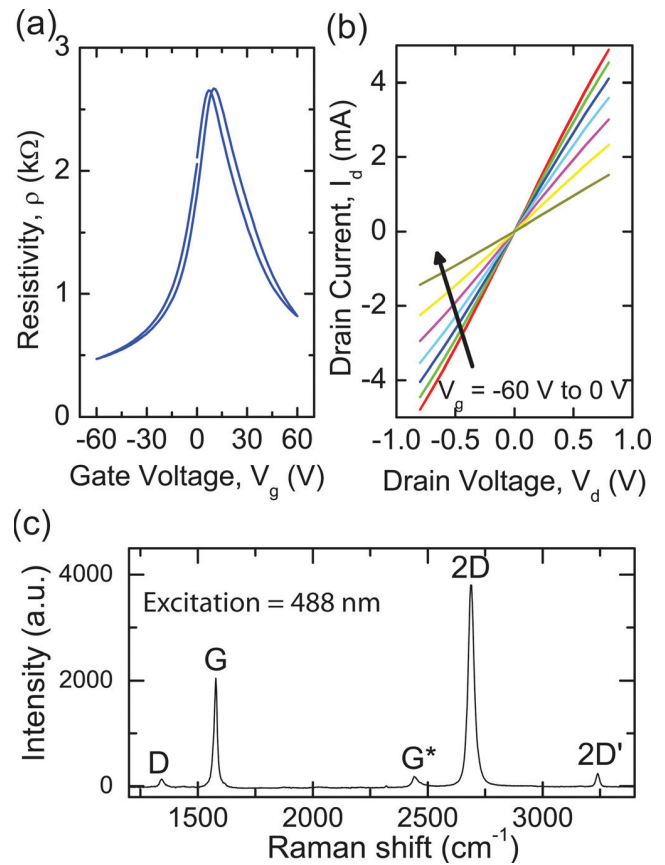


FIG. 1. (a) and (b) Representative room temperature transfer and output curves, respectively, of a CVD graphene device (channel length  $L = 4$   $\mu\text{m}$ , width  $W = 12$   $\mu\text{m}$ ) under vacuum (pressure  $< 10^{-5}$  Torr). (c) Representative Raman spectrum of CVD graphene for a completed device in ambient using 488 nm laser excitation and a 50 $\times$  objective (NA = 0.65). Scattered light is detected with a half-meter Acton SP-2500 spectrometer and Princeton Instruments CCD array.

graphene Raman spectrum shows the D, G, and 2D peak positions at  $\sim 1342$  cm<sup>-1</sup>,  $\sim 1578$  cm<sup>-1</sup>, and  $\sim 2698$  cm<sup>-1</sup>, respectively. The high crystalline quality of the graphene was verified by the ratio of 2D to G peak areas ( $\sim 3.5$ )<sup>25</sup> and the small D to G peak ratio ( $\sim 0.06$ ).<sup>20,25</sup> Subsequent fits of the 2D peak to a single Lorentzian (see Figure S3 in the supplementary materials<sup>22</sup>) confirm that the graphene is single-layer. Additionally, the 2D peak position is blue-shifted from the intrinsic value of 2677 cm<sup>-1</sup>, which may be due to hole doping of the graphene in ambient and dispersion of the 2D peak with excitation wavelength.<sup>25</sup>

Figure 2(a) shows a representative low-frequency noise spectrum for the device presented in Figure 1 (bandwidth = 1–200 Hz for all noise measurements). Empirically, Equation (1) shows that the  $1/f$  noise can be expressed as<sup>26–28</sup>

$$S_I = \left( \frac{\alpha_H}{N} \right) \left( \frac{I^{\gamma}}{f^{\beta}} \right), \quad (1)$$

where  $S_I$  is the current power spectral density,  $I$  is the average current,  $f$  is the frequency,  $N$  is the number of carriers, and  $\alpha_H$  is the Hooge parameter. Ideally, the exponents  $\beta$  and  $\gamma$  are close to 1 and 2, respectively. For representative devices, the exponent  $\beta$  ranges between 1.1 and 1.2 for  $V_g$  varying from

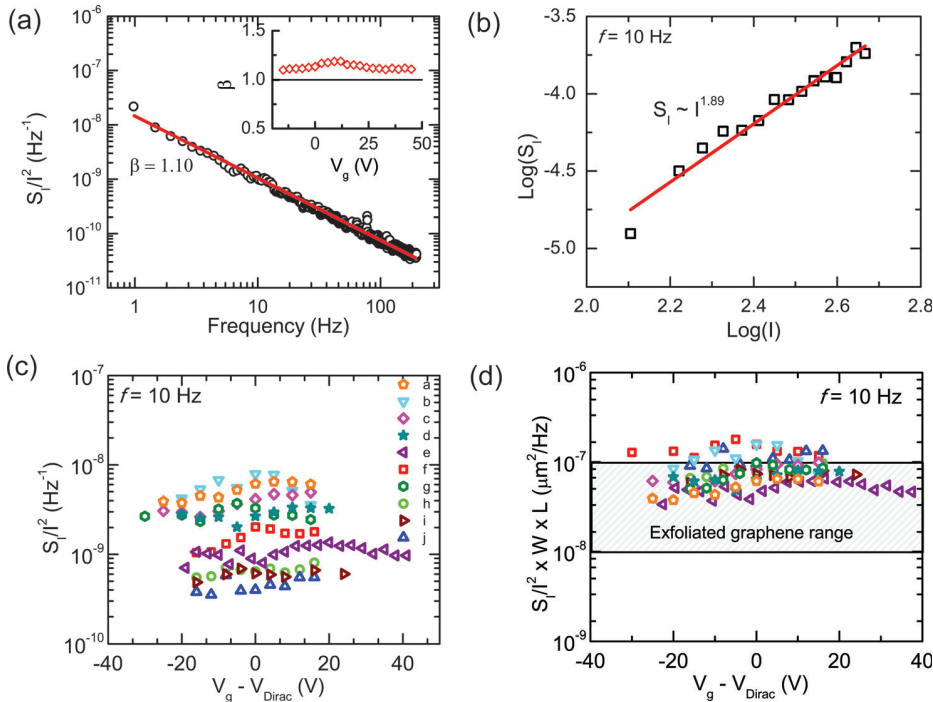


FIG. 2. (a) Noise spectral density ( $S_1/f^2$ ) versus frequency of the device in Figure 1 showing  $1/f^\beta$  behavior with  $\beta = 1.10 \pm 0.01$  at  $V_g = 33$  V and  $V_d = 0.3$  V. The inset shows  $\beta$  extracted from noise spectra taken at different  $V_g$  for the same device. Note: the units of current,  $I$ , are microamperes. (b) Plot of  $\log(S_1)$  versus  $\log(I)$  at  $f = 10$  Hz for the same device measured at  $V_g = 9$  V. The least-square fit line shows the current exponent is  $\gamma = 1.89 \pm 0.09$ . (c) Noise spectral density ( $S_1/f^2$ ) versus ( $V_g - V_{\text{Dirac}}$ ) for all 10G-FETs measured at  $f = 10$  Hz. Channel geometries,  $L$  ( $\mu\text{m}$ )  $\times$   $W$  ( $\mu\text{m}$ ), are: a =  $2 \times 5$ ; b, c =  $4 \times 5$ ; d =  $2 \times 12$ ; e, f, g =  $4 \times 12$ ; h, i =  $4 \times 30$ ; and j =  $4 \times 60$ . (d) The data from (c) are normalized by area,  $(S_1/f^2)(L \times W)$ , and plotted as a function of ( $V_g - V_{\text{Dirac}}$ ). The shaded region indicates noise values typically reported for exfoliated graphene transistors on thermal oxide Si substrates.

–10 to 50 V (inset Figure 2(a)). Indeed,  $\beta$  values for all of the devices fall within 1.05–1.3 at all  $V_g$  values (see Figure S4(a) in the supplementary materials<sup>22</sup>). Additionally,  $\gamma$  for this device is  $\sim 1.89$  (Figure 2(b)), indicating that the  $1/f$  noise is an equilibrium phenomenon.<sup>27</sup> In all 10 of the devices,  $\gamma$  is in the range  $2 \pm 0.2$ , which suggests that the device current fluctuations are caused by variations in resistance and are not due to the applied current (see Figure S4(b) in the supplementary materials<sup>22</sup>).

These observed fluctuations in device current ( $I = eN\mu$ ) can arise from perturbations in either the number of carriers ( $N$ ) or the carrier mobility ( $\mu$ ). Thus, two different models are commonly used to interpret the physical origin of  $1/f$  noise.<sup>29,30</sup> Historically, the carrier number fluctuation model (commonly referred to as the McWhorter model)<sup>31</sup> has been successful in explaining the origin of  $1/f$  noise in metal-oxide-semiconductor FETs,<sup>32</sup> whereas the mobility fluctuation model (i.e., Hooge model) is frequently used to describe low-frequency noise in metal films.<sup>26–28</sup> Typically, the dependence of  $S_1$  on the charge carrier density (which is proportional to  $V_g$ ) is used to distinguish between these noise origin models. However, these two models can be closely related, since fluctuations in the cross-section of scattering centers (i.e., mobility fluctuations) can be due to the capture/release of charge carriers (i.e., carrier number fluctuations) in interfacial trap states. Therefore, a correlated carrier number-mobility fluctuation model<sup>33</sup> was developed to more completely describe  $1/f$  noise in such materials, including graphene.<sup>6,12,13</sup>

The number of carriers ( $N$ ) in a G-FET can be varied either by controlling the channel area or by varying the gate bias  $V_g$  in a field-effect geometry. Figure 2(c) shows the behavior of the normalized noise spectral density ( $S_1/f^2$ ) at  $f = 10$  Hz in all 10 devices with varying channel area ( $10$ – $120 \mu\text{m}^2$ ). In Figure 2(d),  $S_1/f^2$  is scaled by the channel area, which decreases the spread in  $(S_1/f^2)(L \times W)$  over the

entire  $V_g$  range, in agreement with the Hooge mobility fluctuation model ( $S_1/f^2 \sim 1/N$ , assuming weak carrier density dependence on mobility).<sup>16,23,27</sup> However, there is no overriding correlation between  $S_1/f^2$  and  $V_g$ , suggesting that the noise does not strictly follow either of the classic origin models, as will be discussed below. On the other hand, most of our device data fall within the range of values ( $10^{-7}$ – $10^{-8} \mu\text{m}^2/\text{Hz}$ ) observed in high-quality, exfoliated single-layer, and bilayer G-FETs (dashed region in Figure 2(d)).<sup>8,9</sup> Notably, these noise metrics are comparable despite an order of magnitude difference in field-effect mobility between the previous exfoliated graphene reports and our CVD graphene. Furthermore, the noise amplitude ( $A = (1/Z) \sum_{i=1}^Z f_i \times S_{ii}/I^2$ , where  $Z = 400$ ), ranges from  $4 \times 10^{-8}$  to  $10^{-7}$  for all 10 devices, is similar to exfoliated graphene.<sup>6</sup> In contrast, previous CVD graphene studies have reported significantly larger levels of  $1/f$  noise.<sup>8,14,15</sup> For example, in one CVD graphene report, the minimum value of area-normalized ( $S_1/f^2$ ) ( $L \times W$ ) was  $2 \times 10^{-6} \mu\text{m}^2/\text{Hz}$  (at  $f = 10$  Hz).<sup>15</sup> In another CVD graphene study,  $A$  was in the range of  $[3$ – $10] \times 10^{-6}$  at comparable  $V_g$  to the present work.<sup>14</sup> Overall, the noise spectral density in the present CVD G-FETs shows an order of magnitude improvement over these previous reports.

Next, we discuss the dependence of the  $1/f$  noise on carrier density to elucidate its fundamental origin in the present devices. For this analysis, the noise amplitude is utilized instead of the noise spectral density to remove random error that is introduced when selecting  $S_1/f^2$  at a particular frequency. Overall, three qualitatively different  $A$  versus  $V_g$  behaviors are observed in the G-FETs. First, a small subset of the devices shows a weak dependence of  $A$  on  $V_g$  (see Figure S5(a) in the supplementary material<sup>22</sup>), which is attributed to an inhomogeneity of charge distribution that persists in disordered CVD graphene up to large  $V_g$ .<sup>9</sup> Figure 3(a) shows a trend in another subset of devices where the noise amplitude and device resistance decrease together at

all measured  $V_g$  values ( $\Lambda$ -shape), which is qualitatively consistent with the previous observations in exfoliated and CVD graphene.<sup>12,13</sup> The carrier number and mobility fluctuation models predict a dependence of the noise amplitude on carrier density ( $n$ ) as  $1/n^2$  and  $1/n$ , respectively.<sup>27,31</sup> If  $n = \sqrt{n_r^2 + (C_g \cdot (V_g - V_{Dirac})/q)^2}$ , where  $C_g$  is the gate capacitance per unit area,  $n_r$  is the residual carrier density near the Dirac point, and  $q$  is the elementary unit of charge, then both models fit well to the data in this range of  $V_g$ , and the origin of the noise cannot be definitively determined. However, the scaling of the noise spectral density with channel area and correlation between  $A$  and  $R$  ( $V_g$ ) suggests that the Hooge mobility fluctuation model dominates in this subset of devices. Consequently, we extract a Hooge parameter  $\alpha_H$  in the range  $6 \times 10^{-3}$ – $1.1 \times 10^{-2}$ , which is comparable to the previous exfoliated and CVD G-FETs with similar field-effect mobilities.<sup>8,12–14</sup>

The  $1/f$  noise in the final subset of G-FETs (Figure 3(b)) deviates significantly from the Hooge fluctuation model. In these devices, the noise amplitude exhibits a non-monotonic dependence on the gate bias, where  $A$  increases with decreasing  $R$  near the Dirac point and then begins to decrease with decreasing  $R$  when  $V_g > 20$  V. This so-called “M-shape” behavior has also been reported in high-quality single-layer graphene,<sup>13,16–19</sup> suspended single-layer graphene,<sup>13</sup> and bilayer graphene devices.<sup>13</sup> A “V-shape” dependence near the Dirac point was also observed in some of the present devices, but it is likely that this behavior would ultimately become M-shaped at extended  $V_g$  ranges.<sup>9,18</sup> M-shape behavior, which is closely related to the unusual band structure in

graphene, has been described through different but related methods including an augmented charge model,<sup>19</sup> the interplay between short-range defects and long-range Coulomb scatters,<sup>16</sup> and a correlated number-mobility fluctuation/configurational noise model.<sup>13,33,34</sup> We employ the last model here (Equation (2) below) to fit the M-shape dependence.<sup>13</sup> This model defines the noise spectral density as

$$\frac{S_I}{I^2} = B \left( \frac{\partial \sigma}{\partial n} \right)^2 + Ch(n), \quad (2)$$

where  $\sigma$  is graphene conductivity, the parameters  $B$  and  $C$  are independent of  $n$  ( $n = (V_g - V_{Dirac})/q$ ), and the function  $h(n) = |n|^k$  for  $|n| > n_0$ ;  $h(n) = \text{constant}$  for  $|n| < n_0$ .<sup>13</sup> The characteristic carrier density ( $n_0$ ) defines the point of crossover to inhomogeneity in the charge landscape. In Equation (2), the first term results from correlated number-mobility fluctuations<sup>33</sup> and is called the exchange noise ( $N_{ex}$ ). On the other hand, the second term in Equation (2) describes fluctuations in the Coulomb scattering cross-section from the random rearrangement of interfacial trap charges and is called the configurational noise ( $N_{conf}$ ).<sup>34</sup> Figure 3(b) shows a least-squares fit of the data to this model (in red). To obtain this fit to the present data,  $B$ ,  $C$ ,  $n_0$ , and  $k$  as fitting parameters were used, and the electron and hole branches were considered separately. Notably, the best fit exponent  $k = -1$  confirms that the present CVD graphene is single-layer, since  $k > 0$  is observed for thicker graphene samples.<sup>13</sup> From this analysis, it was determined that  $N_{ex}$  dominates the overall  $1/f$  noise for  $|n| < n_0$  and  $N_{conf}$  dominates for  $|n| > n_0$ , where  $n_0 \sim 1.3 \times 10^{12} \text{ cm}^{-2}$  for electrons and  $n_0 \sim 1.1 \times 10^{12} \text{ cm}^{-2}$  for holes. These values of  $n_0$  agree well with the value of critical carrier density at which the dominant scattering mechanism crosses over from long range to short range, as extracted in an earlier study on charge transport in devices fabricated following a similar protocol.<sup>35</sup> Lastly, we did not find any correlation between channel geometry and noise models. Among a total of 10 measured devices, devices b, f, and g (see Figure 2(c) caption for channel geometries) followed the Hooge model, while the rest of the devices followed the correlated number-mobility fluctuation model.

It should be noted that  $N_{conf}$  is significantly reduced near the Dirac point in the present CVD G-FETs, in contrast to the previous CVD graphene reports where  $N_{conf}$  dominates at all  $V_g$ .<sup>13</sup> Prior to this study, a similar lowering of  $N_{conf}$  had only been achieved in suspended single-layer graphene devices, which reduce interfacial disorder by eliminating the substrate, and bilayer G-FETs, where the first graphene layer screens trapped charges in the gate oxide.<sup>13</sup> However, the M-shape dependence in supported single-layer G-FETs has not been analyzed within this framework, and a direct comparison of  $N_{conf}$  between supported exfoliated graphene and transferred CVD graphene is not possible.<sup>16,19</sup> Therefore, we propose that the reduced noise in the present CVD G-FETs results from the relative inability of trapped charges to redistribute dynamically at a timescale longer than 5 ms ( $1/200 \text{ Hz}^{-1}$ ). This reduced interfacial charge disorder can likely be attributed to the device processing protocol that avoids aqueous treatments following graphene transfer, since water has been shown to contribute to long-range scattering, which in turn increases  $1/f$  noise in graphene devices.<sup>17</sup>

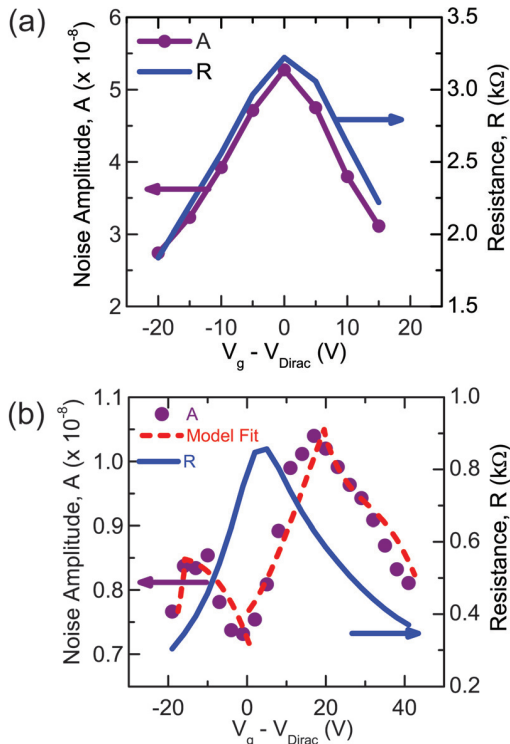


FIG. 3. (a) Experimental Hooge dependence of the noise amplitude ( $A$ ) versus  $V_g$  for a CVD graphene device with  $L = 4 \mu\text{m}$  and  $W = 5 \mu\text{m}$ . (b) Experimental M-shape dependence of  $A$  versus  $V_g$  for the graphene device of Figure 1.

Meanwhile, the dominance of  $N_{\text{ex}}$  at low  $V_g$  suggests that the remaining  $1/f$  noise in the present devices results from capture-emission processes of relatively “fixed” trapped charges in the dielectric or remnant residues.

In conclusion, by avoiding post-transfer aqueous processing, we have achieved an order of magnitude reduction of  $1/f$  noise in CVD G-FETs. The area-normalized noise spectral density ( $10^{-7}$ – $10^{-8}$   $\mu\text{m}^2 \text{Hz}^{-1}$ ) is comparable to high-quality exfoliated graphene and Si-based FETs at similar carrier density. Since no obvious correlation is found between the noise amplitude and gate bias dependence, both the Hooge mobility fluctuation model and correlated carrier-mobility fluctuation model were used to describe the qualitatively different behaviors observed in these devices. Using these models, the overall reduction of noise in these devices is attributed to a decrease in the configurational noise, which is achieved by quenching dynamic redistribution of interfacial disorder. Moreover, the lack of correlation between the Hooge parameter and the carrier mobility suggests that additional improvements in CVD growth to minimize crystal defects are unlikely to produce quieter graphene devices. Instead, strategies that have been employed to reduce the noise in high-quality exfoliated graphene may prove effective in diminishing  $1/f$  noise in CVD graphene. In this manner, this study will inform ongoing efforts to improve the performance of RF and related graphene-based electronic devices.

This work was supported by the Northwestern University Materials Research Science and Engineering Center (NSF DMR-1121262) and the Defense Threat Reduction Agency MIPR No. 15-15399. H.N.A. acknowledges support from a NASA Space Technology Research Fellowship (NSTRF No. NNX11AM87H), and K.A.L. acknowledges support from the NSF Graduate Research Fellowship Program. This research was performed while S.W.S. held a National Research Council Associateship Award at the Naval Research Laboratory.

<sup>1</sup>D. Jariwala, V. K. Sangwan, L. J. Lauhon, T. J. Marks, and M. C. Hersam, *Chem. Soc. Rev.* **42**, 2824 (2013).

<sup>2</sup>F. Schwierz, *Nat. Nanotechnol.* **5**, 487 (2010).

<sup>3</sup>K. S. Novoselov, D. Jiang, F. Schedin, T. J. Booth, V. V. Khotkevich, S. V. Morozov, and A. K. Geim, *Proc. Natl. Acad. Sci. U.S.A.* **102**, 10451 (2005).

<sup>4</sup>C. Smith, R. Qaisi, Z. Liu, Q. Yu, and M. M. Hussain, *ACS Nano* **7**, 5818 (2013).

<sup>5</sup>W. Gannett, W. Regan, K. Watanabe, T. Taniguchi, M. F. Crommie, and A. Zettl, *Appl. Phys. Lett.* **98**, 242105 (2011).

<sup>6</sup>S. Bae, H. Kim, Y. Lee, X. Xu, J.-S. Park, Y. Zheng, J. Balakrishnan, T. Lei, H. Ri Kim, Y. I. Song, Y.-J. Kim, K. S. Kim, B. Ozyilmaz, J.-H. Ahn, B. H. Hong, and S. Iijima, *Nat. Nanotechnol.* **5**, 574 (2010).

<sup>7</sup>F. Bonaccorso, A. Lombardo, T. Hasan, Z. Sun, L. Colombo, and A. C. Ferrari, *Mater. Today* **15**, 564 (2012).

<sup>8</sup>A. A. Balandin, *Nat. Nanotechnol.* **8**, 549 (2013).

<sup>9</sup>S. Ruyantsev, G. Liu, W. Stillman, M. Shur, and A. A. Balandin, *J. Phys.: Condens. Matter* **22**, 395302 (2010).

<sup>10</sup>Z. Cheng, Q. Li, Z. Li, Q. Zhou, and Y. Fang, *Nano Lett.* **10**, 1864 (2010).

<sup>11</sup>G. Liu, S. Ruyantsev, M. Shur, and A. A. Balandin, *Appl. Phys. Lett.* **100**, 033103 (2012).

<sup>12</sup>Y.-M. Lin and P. Avouris, *Nano Lett.* **8**, 2119 (2008).

<sup>13</sup>A. N. Pal, S. Ghatak, V. Kochat, E. S. Sneha, A. Sampathkumar, S. Raghavan, and A. Ghosh, *ACS Nano* **5**, 2075 (2011).

<sup>14</sup>A. N. Pal, A. A. Bol, and A. Ghosh, *Appl. Phys. Lett.* **97**, 133504 (2010).

<sup>15</sup>S. K. Lee, C. G. Kang, Y. G. Lee, C. Cho, E. Park, H. J. Chung, S. Seo, H.-D. Lee, and B. H. Lee, *Carbon* **50**, 4046 (2012).

<sup>16</sup>Y. Zhang, E. E. Mendez, and X. Du, *ACS Nano* **5**, 8124 (2011).

<sup>17</sup>A. A. Kaverzin, A. S. Mayorov, A. Shytov, and D. W. Horsell, *Phys. Rev. B* **85**, 075435 (2012).

<sup>18</sup>G. Xu, C. M. Torres, Y. Zhang, F. Liu, E. B. Song, M. Wang, Y. Zhou, C. Zeng, and K. L. Wang, *Nano Lett.* **10**, 3312 (2010).

<sup>19</sup>I. Heller, S. Chatoor, J. Männik, M. A. G. Zevenbergen, J. B. Oostinga, A. F. Morpurgo, C. Dekker, and S. G. Lemay, *Nano Lett.* **10**, 1563 (2010).

<sup>20</sup>X. Li, C. W. Magnuson, A. Venugopal, R. M. Tromp, J. B. Hannon, E. M. Vogel, L. Colombo, and R. S. Ruoff, *J. Am. Chem. Soc.* **133**, 2816 (2011).

<sup>21</sup>J. T. Robinson, S. W. Schmucker, C. B. Diaconescu, J. P. Long, J. C. Culbertson, T. Ohta, A. L. Friedman, and T. E. Beechem, *ACS Nano* **7**, 637 (2013).

<sup>22</sup>See supplementary material at <http://dx.doi.org/10.1063/1.4942468> for atomic force microscopy images, fit of the graphene 2D Raman peak to a single Lorentzian, and additional transport and noise characteristics of the G-FETs.

<sup>23</sup>V. K. Sangwan, H. N. Arnold, D. Jariwala, T. J. Marks, L. J. Lauhon, and M. C. Hersam, *Nano Lett.* **13**, 4351 (2013).

<sup>24</sup>V. K. Sangwan, D. Jariwala, K. Everaerts, J. J. Mcmorrow, J. He, M. Grayson, L. J. Lauhon, T. J. Marks, and M. C. Hersam, *Appl. Phys. Lett.* **104**, 083503 (2014).

<sup>25</sup>J. E. Lee, G. Ahn, J. Shim, Y. S. Lee, and S. Ryu, *Nat. Commun.* **3**, 1024 (2012).

<sup>26</sup>F. N. Hooge, *Phys. Lett. A* **29**, 139 (1969).

<sup>27</sup>P. Dutta and P. M. Horn, *Rev. Mod. Phys.* **53**, 497 (1981).

<sup>28</sup>F. N. Hooge, *IEEE Trans. Electron Devices* **41**, 1926 (1994).

<sup>29</sup>L. K. J. Vandamme, X. S. Li, and D. Rigaud, *IEEE Trans. Electron Devices* **41**, 1936 (1994).

<sup>30</sup>K. K. Hung, P. K. Ko, H. Chenming, and Y. C. Cheng, *IEEE Trans. Electron Devices* **37**, 654 (1990).

<sup>31</sup>A. L. McWhorter and R. H. Kingston, *Semiconductor Surface Physics* (University of Pennsylvania Press, 1957).

<sup>32</sup>Z. Celik-Butler and T. Y. Hsiang, *Solid State Electron.* **30**, 419 (1987).

<sup>33</sup>R. Jayaraman and C. G. Sodini, *IEEE Trans. Electron Devices* **36**, 1773 (1989).

<sup>34</sup>J. Pelz and J. Clarke, *Phys. Rev. B* **36**, 4479 (1987).

<sup>35</sup>C. D. Cress, J. G. Champlain, I. S. Esqueda, J. T. Robinson, A. L. Friedman, and J. J. Mcmorrow, *IEEE Trans. Nucl. Sci.* **59**, 3045 (2012).